JOURNAL OF GUIDANCE, CONTROL, AND DYNAMICS
Vol. 18, No. 2, March–April 1995

Optimal Guidance and Nonlinear Estimation for Interception of Decelerating Targets

Michael E. Hough*
Textron Defense Systems, Wilmington, Massachusetts 01887

Optimal guidance and nonlinear estimation algorithms are formulated for interception of a nonmaneuvering target vehicle decelerated by atmospheric drag. For an interceptor with two-axis control of translational acceleration, time-to-go may be selected to generate a zero-acceleration command along the uncontrolled axis. A nine-state, extended Kalman filter is formulated in relative-motion coordinates, and the target deceleration vector is modeled by a linear, first-order process. With angle measurements from a strapdown seeker, very small miss distances can be achieved, despite large estimation errors in range, because of the time-to-go algorithm. Theoretical collision probabilities are determined, using Monte Carlo simulations, as functions of sensor measurement accuracy, filter update rate, and engagement crossing angle.

I. Introduction

SMALL, kinetic-kill vehicles (KKVs) are presently being considered for ground-based defensive systems.[1] Preliminary design trades indicate that very accurate sensors, fast update rates, and fast response times are required to maximize probability of collision.[2]

The KKV guidance system will implement modern guidance and estimation algorithms in a microprocessor. By processing inertial-navigation measurements and seeker measurements, the estimation algorithm generates estimates of the target state vector. With these estimates, the guidance algorithm generates acceleration commands to a translation-control system that maneuvers the KKV toward the target. An attitude-control system stabilizes the vehicle at zero angle of attack to minimize parasitic lift accelerations and distortion of the seeker measurements. Translation-control and attitude-control forces are generated by propulsive systems, which are preferred for rapid response.

For continuous, linear systems with process and measurements containing white noise, the translation-control (or guidance) algorithm and estimation algorithm may be formulated independently. With a quadratic performance index, the optimal (deterministic) control is a linear function of the state variables. In the stochastic case, the optimal control is a linear function of the maximum-likelihood estimates of the state variables.

Optimal-guidance algorithms minimize miss distance and integral-square acceleration.[3] Although engagement final time T is generally a free parameter, T may be specified by including it in the cost function.[4,5] A simplified form of optimal guidance is proportional guidance, which has been implemented for interception of nonmaneuvering targets[6–8] and maneuvering targets with constant acceleration.[9,10]

Several techniques are available for nonlinear estimation of the relative-motion trajectory. These techniques include minimum-variance estimation, estimation by statistical linearization, and batch least-squares estimation.[11,12] The simplest implementation of minimum-variance estimation is the extended Kalman filter (EKF). This technique has been applied extensively to interception problems.[13–16]

In this article, optimal-guidance and nonlinear estimation algorithms are formulated for interception of a nonmaneuvering target vehicle decelerated by atmospheric drag. As solutions of the optimal-control and estimation problems are well known, emphasis is placed on the implementation of the simplest, yet most accurate, optimal-guidance and estimation algorithms. Two contributions are concerned with 1) a new algorithm for specifying time to go, which has surprising advantages from a filtering standpoint, and 2) a new EKF model for target deceleration.

A summary of the presentation of this article is as follows:

In Sec. II the equations of relative motion are formulated in vector form. These equations are the basis for the optimal-guidance and nonlinear estimation algorithms. Section III formulates an optimal-guidance algorithm for three-axis control of translational acceleration, with perturbations arising from a variable disturbing acceleration. With two-axis control, time to go may be selected to generate a zero-acceleration command along the uncontrolled axis. Analytic solutions of the relative-motion equations demonstrate convergence of the intercept trajectory, with two-axis control.

For filtering purposes, a linear dynamics model of the engagement is formulated in relative-motion coordinates in Sec. IV. Over short time intervals, the target deceleration vector may be approximated by a linear, first-order process. Section V formulates a nine-state EKF in a Cartesian-inertial frame. The states include the relative-position vector, relative-velocity vector, and the absolute-acceleration vector of the target vehicle. The EKF dynamics model is linear in the state variables. Seeker-angle measurements are nonlinear functions of the state variables.

Section VI evaluates statistical properties of the EKF by Monte Carlo simulation of the EKF and its nonlinear "truth" model. Brief descriptions are presented of the simulation and its preprocessing algorithms. Section VII considers the performance of the filter. Although certain states are unobservable with angle measurements, filter estimates do not diverge because of very accurate angle measurements, high update rates of the EKF, "self-consistent" initialization of the EKF, and a good model of target deceleration. Surprisingly, very small miss distances can be achieved, despite large estimation errors in range, because of the time-to-go algorithm. Section VIII determines theoretical limits on collision probability by Monte Carlo simulation. Sensitivities are specified to sensor measurement accuracy, EKF update rate, and trajectory crossing angle.

II. Equations of Relative Motion

Two dynamic systems with six degrees of freedom describe the coupled translational and rotational motions of an interceptor (the "pursuer") and a nonmaneuvering, but decelerating, target vehicle (the "evader"). The equations of relative motion are determined from the translational dynamics of both vehicles.

The pursuer is actively controlled using propulsive systems that independently generate translation-control forces and attitude-control forces. Using acceleration commands generated by a guid-

Received June 15, 1993; revision received March 18, 1994; accepted for publication May 2, 1994.

*Principal Scientist. Member AIAA.

ance algorithm, translation-control forces are commanded in body yz axes, orthogonal to the longitudinal x-axis. These forces cause the velocity vector to rotate away from the longitudinal axis, inducing angle of attack and lift acceleration in the *opposite* direction. To reduce the (unwanted) lift acceleration, the attitude-control system stabilizes the vehicle near zero angle of attack. Using force commands generated by an autopilot algorithm, attitude-control forces are commanded in body yz axes.

The evader, which is not actively controlled, is spin stabilized and decelerated by aerodynamic drag. At a nonzero angle of attack, lift acceleration generates a helical motion of the evader center of mass about its (mean) velocity vector. In this article, these motions are suppressed intentionally, by judicious selection of initial conditions (i.e., small angles of attack).

Translational motions of each vehicle may be described by two dynamic systems with three degrees of freedom:

$$\overset{I}{\boldsymbol{v}}_p = \boldsymbol{a}_c + \boldsymbol{a}_p + \boldsymbol{g}_p, \qquad \overset{I}{\boldsymbol{r}}_p = \boldsymbol{v}_p \tag{1}$$

$$\overset{I}{\boldsymbol{v}}_e = \boldsymbol{a}_e + \boldsymbol{g}_e, \qquad \overset{I}{\boldsymbol{r}}_e = \boldsymbol{v}_e \tag{2}$$

where all vectors are resolved in an inertial frame unless otherwise indicated. Superscript I indicates time derivatives taken with respect to an inertial frame. Subscripts usually identify the vehicle, as in the case of the position and velocity vectors, indicated by $\boldsymbol{r}_p, \boldsymbol{v}_p$ and $\boldsymbol{r}_e, \boldsymbol{v}_e$. Resultant accelerations include gravitational accelerations $\boldsymbol{g}_p, \boldsymbol{g}_e$, aerodynamic accelerations $\boldsymbol{a}_p, \boldsymbol{a}_e$, and a control acceleration $\boldsymbol{a}_c$ for the pursuer.

For the pursuer, independent propulsive systems generate translation-control and attitude-control forces in body yz axes. Each force component is modeled by a first-order process, with time constant τ_p:

$$\dot{F}_{c,i} = (1/\tau_p)(F^*_{c,i} - F_{c,i}) \qquad \text{for} \qquad i = y, z$$

Each force command $F^*_{c,i}$ is saturation limited. For example, translation-control commands are generated in body yz axes, from an acceleration command $\boldsymbol{a}^*_c$, in inertial axes:

$$\tilde{\boldsymbol{F}}^*_c = \mathcal{R}\boldsymbol{F}^*_c, \qquad \boldsymbol{F}^*_c = m_p \boldsymbol{a}^*_c$$

where $\mathcal{R}$ is the rotation matrix from inertial to body axes. The guidance algorithm specifies $\boldsymbol{a}^*_c$ to achieve intercept. Attitude-control commands are generated in body axes directly.

Attitude motions of both vehicles are determined by Euler's equations of motion and kinematic equations. For the pursuer, the solutions of Euler's equations specify the inertial angular rate generated by control torques and aerodynamic torques. Solutions of the kinematic equations specify the Euler angles that define the rotation matrix $\mathcal{R}$. Similar considerations apply to the evader, except that this vehicle is not actively controlled.

Optimal-guidance and nonlinear estimation algorithms will be formulated in relative-motion coordinates. Position and velocity vectors of the evader relative to the pursuer are defined by

$$\boldsymbol{r} = \boldsymbol{r}_e - \boldsymbol{r}_p, \qquad \boldsymbol{u} = \boldsymbol{v}_e - \boldsymbol{v}_p$$

By subtracting Eq. (2) from Eq. (1), it follows that

$$\overset{I}{\boldsymbol{u}} = -\boldsymbol{a}_c + \boldsymbol{g}_e - \boldsymbol{g}_p + \boldsymbol{a}_e - \boldsymbol{a}_p, \qquad \overset{I}{\boldsymbol{r}} = \boldsymbol{u}$$

The following approximations will simplify the formulations:

1) For close encounters, the evader gravitational acceleration may be expanded in a series about the pursuer gravitational acceleration:

$$\boldsymbol{g}_e \cong \boldsymbol{g}_p + \Gamma_p \boldsymbol{r} + \text{hot}, \qquad \Gamma_p = \frac{\partial \boldsymbol{g}_p}{\partial \boldsymbol{r}_p}$$

where Γ_p is the gravity-gradient matrix evaluated at $\boldsymbol{r}_p$. When higher order terms are neglected, the equations of relative motion may be expressed by

$$\overset{I}{\boldsymbol{u}} = -\boldsymbol{a}_c + \Gamma_p \boldsymbol{r} + \boldsymbol{a}_e - \boldsymbol{a}_p, \qquad \overset{I}{\boldsymbol{r}} = \boldsymbol{u} \tag{3}$$

2) When both vehicles have zero angles of attack, a disturbance acceleration arises from aerodynamic drag on both vehicles

$$\boldsymbol{a}_d = \boldsymbol{a}_e - \boldsymbol{a}_p \tag{4a}$$

$$\boldsymbol{a}_p = -\tfrac{1}{2} b_p u_p \boldsymbol{u}_p, \qquad b_p = \frac{C_{x,p} A_p \rho_p}{m_p}$$
$$\boldsymbol{u}_p = \boldsymbol{v}_p - \boldsymbol{\omega}_\oplus \times \boldsymbol{r}_p \tag{4b}$$

$$\boldsymbol{a}_e = -\tfrac{1}{2} b_e u_e \boldsymbol{u}_e, \qquad b_e = \frac{C_{x,p} A_e \rho_e}{m_e}$$
$$\boldsymbol{u}_e = \boldsymbol{v}_e - \boldsymbol{\omega}_\oplus \times \boldsymbol{r}_e \tag{4c}$$

where $\boldsymbol{u}_p, \boldsymbol{u}_e$ are the velocity vectors relative to Earth's atmosphere rotating with angular velocity $\boldsymbol{\omega}_\oplus$. The parameters b_p, b_e depend on vehicle reference areas A_p, A_e, masses m_p, m_e, axial-force coefficients $C_{x,p}, C_{x,e}$, and air densities ρ_p, ρ_e. At zero angles of attack, $C_{x,p}, C_{x,e}$ are nonlinear functions of the Mach numbers and Reynolds numbers of both vehicles. Air densities are nonlinear functions of vehicle altitudes.

The simplified equations (3), with variable disturbance acceleration (4), will be used to formulate optimal-guidance and nonlinear estimation algorithms as follows.

III. Optimal Guidance for Target Intercept

An optimal-guidance algorithm may be formulated for a pursuer with three-axis control of translational acceleration in the inertial frame. Certain simplifications are necessary for a tractable solution. When gravity-gradient accelerations are neglected and acceleration commands are executed instantaneously ($\boldsymbol{a}_c = \boldsymbol{a}^*_c$), the equations of relative motion (3) may be expressed by

$$\overset{I}{\boldsymbol{u}} = -\boldsymbol{a}^*_c + \boldsymbol{a}_d, \qquad \overset{I}{\boldsymbol{r}} = \boldsymbol{u} \tag{5}$$

A variable disturbance acceleration $\boldsymbol{a}_d$ arises from aerodynamic drag (4) on both vehicles. The acceleration command $\boldsymbol{a}^*_c$ may be selected to minimize the cost function with constant penalties c, b on integral-square acceleration and miss distance $\boldsymbol{r}(T)$ at the engagement final time T:

$$J = \frac{1}{2} b \boldsymbol{r}(T) \cdot \boldsymbol{r}(T) + \frac{1}{2} \int_0^T \frac{\boldsymbol{a}^*_c \cdot \boldsymbol{a}^*_c}{c}\, \mathrm{d}t$$

An optimal solution may be determined using the calculus of variations (refer to the Appendix):

$$\boldsymbol{a}^*_c(\tau) = K(\tau)[\boldsymbol{r}(\tau) + \tau \boldsymbol{u}(\tau) + \tau \eta(\tau) - \rho(\tau)]$$

$$\tau = T - t, \qquad K(\tau) = \frac{3bc\tau}{3 + bc\tau^3}$$

$$\eta(\tau) = \int_0^\tau \boldsymbol{a}_d(s)\, \mathrm{d}s, \qquad \rho(\tau) = \int_0^\tau \eta(s)\, \mathrm{d}s$$

Two simplifications will be implemented:

1) The optimal gain is independent of b, c in the "zero-miss" limit:

$$\lim_{b \to \infty} [K(\tau)] = \frac{3}{\tau^2}$$

2) After integration by parts, the quadratures may be approximated by

$$\eta(\tau) \cong \tau \boldsymbol{a}_d(\tau) + \text{hot}, \qquad \rho(\tau) \cong \tfrac{1}{2}\tau^2 \boldsymbol{a}_d(\tau) + \text{hot}$$

After simplification, the optimal solution may be expressed by

$$\boldsymbol{a}^*_c(\tau) = \frac{3}{\tau^2}\left[\boldsymbol{r}(\tau) + \tau \boldsymbol{u}(\tau) + \tfrac{1}{2}\tau^2 \boldsymbol{a}_d(\tau)\right] \tag{6}$$

Effectively, the "zero-effort miss," which is the quantity in brackets, is computed as if $\boldsymbol{a}_d$ were a constant vector. This approximation is adequate, provided $\boldsymbol{a}_c^*$ is updated frequently during an engagement. For $\boldsymbol{a}_d = 0$, it may be shown that Eq. (6) is equivalent to proportional guidance.[3,6–8]

The optimal solution (6) may be implemented as an acceleration command to a propulsive divert system with three-axis control. The following vectors may be resolved into components in an inertial frame

$$\boldsymbol{r} = \begin{bmatrix} x \\ y \\ z \end{bmatrix}, \qquad \boldsymbol{u} = \begin{bmatrix} \dot{x} \\ \dot{y} \\ \dot{z} \end{bmatrix}, \qquad \boldsymbol{a}_d = \begin{bmatrix} a_1 \\ a_2 \\ a_3 \end{bmatrix}$$

Following substitution of these identities in Eq. (6), the equations of motion (5) may be expressed in component form:

$$\ddot{x} = a_1 - (3/\tau^2)\left(x + \tau\dot{x} + \tfrac{1}{2}a_1\tau^2\right) \tag{7a}$$

$$\ddot{y} = a_2 - (3/\tau^2)\left(y + \tau\dot{y} + \tfrac{1}{2}a_2\tau^2\right) \tag{7b}$$

$$\ddot{z} = a_3 - (3/\tau^2)\left(z + \tau\dot{z} + \tfrac{1}{2}a_3\tau^3\right) \tag{7c}$$

For constant values of a_1, a_2, a_3, it may be shown that all three components of $\boldsymbol{r}(T)$ converge to zero, assuming perfect information.

For a two-axis control system, time to go may be selected to generate a zero-acceleration command along the uncontrolled axis. With this approach, the collision is shifted along the evader trajectory. For example, when acceleration control is available along the inertial yz axes, τ may be chosen to null the zero-effort miss along the uncontrolled x axis:

$$x(T) = x + \tau\dot{x} + \tfrac{1}{2}a_1\tau^2 = 0$$

For $a_1 > 0$, the smaller of the two real roots is selected:

$$\tau = h(x, \dot{x}) = \min\left[-\frac{\dot{x}}{a_1} \pm \sqrt{\left(\frac{\dot{x}}{a_1}\right)^2 - \frac{2x}{a_1}}\right] \tag{8}$$

Following substitution of Eq. (8) in Eqs. (7), it follows that

$$\ddot{x} = a_1, \qquad \ddot{y} = a_2 - 3\left(\frac{y}{h^2} + \frac{\dot{y}}{h} + \frac{1}{2}a_2\right)$$

$$\ddot{z} = a_3 - 3\left(\frac{z}{h^2} + \frac{\dot{z}}{h} + \frac{1}{2}a_3\right) \tag{9}$$

It will be shown that all three components of $\boldsymbol{r}(T)$ converge to zero simultaneously, for constant values of a_1, a_2, a_3.

Solutions along the uncontrolled x axis may be expressed by

$$x(t) = x_0 + \dot{x}_0 t + \tfrac{1}{2}a_1 t^2, \qquad \dot{x}(t) = \dot{x}_0 + a_1 t$$

where x_0, $\dot{x}_0$ are initial conditions and $x(T) = 0$ because of Eq. (8). By elimination of the time variable, it may be shown that

$$\tfrac{1}{2}\dot{x}^2 - a_1 x = C, \qquad C = \tfrac{1}{2}\dot{x}_0^2 - a_1 x_0$$

Using this result, velocity may be expressed by a function of position:

$$\dot{x} = u(x) = \text{sign}\{\dot{x}_0\}\sqrt{2(C + a_1 x)} \tag{10}$$

For short-duration engagements, $\dot{x}$ has the same algebraic sign as $\dot{x}_0$. Following substitution of Eq. (10) in Eq. (8), it is found that h may be simplified:

$$\tau = h(x) = \min\left(-\frac{u(x)}{a_1} \pm \frac{\sqrt{2C}}{a_1}\right) \tag{11}$$

Solutions along the controlled axes may be expressed by geometric curves $y = f(x)$ and $z = F(x)$. As the two axes are uncoupled, the solutions have a similar form, and only one curve need be considered. For example, total derivatives may be expressed by the chain rule:

$$\dot{y} = f'\dot{x}, \qquad \ddot{y} = f'\ddot{x} + f''\dot{x}^2$$

where primes indicate derivatives with respect to x, $\dot{x}$ is specified by Eq. (10), and $\ddot{x} = a_1$. Following substitution of these identities in Eq. (9), $f(x)$ is specified by a linear, second-order differential equation with variable coefficients:

$$u^2 f'' + \left(a_1 + 3\frac{u}{h}\right)f' + \frac{3}{h^2}f + \tfrac{1}{2}a_2 = 0 \tag{12}$$

The coefficients of Eq. (12) depend on two functions $u(x)$, $h(x)$ specified by Eqs. (10) and (11), respectively. When $\dot{x}_0 < 0$, it follows that

$$u(x) = -\sqrt{2C}\sqrt{1 + \varepsilon x}, \qquad h(x) = -\frac{\sqrt{2C}}{a_1}(1 - \sqrt{1 + \varepsilon x})$$

$$\varepsilon = \frac{a_1}{C}$$

As ε is generally a very small quantity, the coefficients of Eq. (12) may be approximated by power-series expansions in εx, with linear terms retained:

$$\frac{u}{h} \cong \frac{-2C}{x}\left(1 + \tfrac{3}{4}\varepsilon x + \mathcal{O}(\varepsilon^2 x^2)\right)$$

$$\frac{1}{h^2} \cong \frac{2C}{x^2}\left(1 + \tfrac{1}{2}\varepsilon x + \mathcal{O}(\varepsilon^2 x^2)\right)$$

Following substitution of these identities in Eq. (12), it follows that

$$[1 + \varepsilon x]f'' + \left[\frac{1}{2}\varepsilon - \frac{3}{x}\left(1 + \frac{3}{4}\varepsilon x\right)\right]f'$$

$$+ \left[\frac{3}{x^2}\left(1 + \frac{1}{2}\varepsilon x\right)\right]f + \frac{a_2}{4C} = 0 \tag{13}$$

Solutions of Eq. (13) may be expressed by power series with constant coefficients:

$$f(x) = \sum_{m\geq 0} f_m x^m, \qquad f'(x) = \sum_{m\geq 0} m f_m x^{m-1}$$

$$f''(x) = \sum_{m\geq 0} m(m-1) f_m x^{m-2}$$

Following substitution of these identities in Eq. (13), it is found that

$$\sum_{m\geq 0}(m-3)(m-1) f_m x^{m-2}$$

$$+ \frac{1}{4}\varepsilon \sum_{m\geq 0}(4m-3)(m-2) f_m x^{m-1} + \frac{a_2}{4C} = 0$$

By equating coefficients of similar algebraic terms, it may be shown that

$$f_0 = 0, \qquad f_2 = \frac{1}{4}\left(\frac{a_2}{C} - \varepsilon f_1\right)$$

$$f_{m+2} = -\frac{\varepsilon(4m+1)}{4(m+1)} f_{m+1} \qquad \text{for} \qquad m \geq 2$$

where f_1, f_3 are arbitrary constants, specified by initial condi-

tions. Collecting terms, the complete solution of Eq. (13) may be expressed by

$$y = f(x)$$
$$= f_1 x + \frac{a_2 - a_1 f_1}{4C} x^2 + f_3 x^3 + \sum_{m \geq 2} f_{m+2} x^{m+2}$$

At $t = T$, the geometric trajectory passes through the origin because

$$x(T) = 0, \qquad y(T) = f[x(T)] = 0$$

Similar conclusions pertain to $z = F(x)$. Thus, convergence of the intercept trajectory with two-axis control in the inertial frame has been demonstrated. In the actual implementation of Eq. (6), two-axis control is performed in the body frame (rather than inertial frame). As the pursuer is controlled to zero angle of attack, these conclusions are not expected to change because the rotation of the flight path is small.

IV. Filter Dynamics Model

An important design issue is the selection of a coordinate system for the estimation algorithm.[17–19] Ideally, the measurement and dynamic equations should be linear functions of the state variables. In an inertial frame, the relative-motion equations (3) and (4) are linear, but the measurement equations are nonlinear, for a strapdown seeker. The former consideration is important for accurate prediction of the position of the target and filter covariance.

A linear dynamics model of the engagement may be formulated from the equations of relative motion (3) and (4):

$$\overset{I}{\boldsymbol{r}} = \boldsymbol{u}, \qquad \overset{I}{\boldsymbol{u}} = \Gamma_p \boldsymbol{r} + \boldsymbol{a}_e - \boldsymbol{a}_p - \boldsymbol{a}_c \tag{14}$$

Evader and pursuer drag accelerations $\boldsymbol{a}_e$, $\boldsymbol{a}_p$ and pursuer control acceleration $\boldsymbol{a}_c$ are resolved into components in the inertial frame. The gravity-gradient matrix $\Gamma_p(t)$ is evaluated on the pursuer trajectory.

Additional differential equations characterize the time rates of change of the components of $\boldsymbol{a}_e$, since these are treated as filter state variables. Referring to Eq. (4), $\boldsymbol{a}_e$ is a nonlinear function of evader position and velocity:

$$\boldsymbol{a}_e = -\tfrac{1}{2} b_e u_e \boldsymbol{u}_e$$

With this representation, additional state variables would be required to describe the time rates of change of b_e, $\boldsymbol{u}_e$. However, for limited time intervals, a simpler model may be specified by a first-order process:

$$\overset{I}{\boldsymbol{a}}_e = \beta_e \boldsymbol{a}_e \tag{15}$$

The constant parameter β_e models the exponential change in dynamic pressure along the evader trajectory. For descending trajectories, $\beta_e > 0$ because dynamic pressure increases along the path. A nominal trajectory is implicit in the numerical values of β_e and $\boldsymbol{a}_e(0)$.

The approximate model (15) is a minimal representation because evader position and velocity states are not required to characterize $\boldsymbol{a}_e$ and its time derivative. Moreover, the model (15) is linear in the (chosen) state variables. However, it is important to remember that the model (15) is accurate for limited time intervals when the vehicle is at zero angle of attack.

More complicated models would be required to characterize an evader generating lift and control accelerations. For example, sinusoidal lift accelerations would be generated by a spinning (ballistic) vehicle at nonzero angles of attack. In this case, the mean acceleration would be described by Eq. (15), but additional states would be required to characterize the helical motion of the center of mass about the mean trajectory.

Nine elements of the state vector $\boldsymbol{x}$ are the components of $\boldsymbol{r}$, $\boldsymbol{u}$, and $\boldsymbol{a}_e$, resolved along axes that are fixed in the inertial frame:

$$\boldsymbol{x} = \begin{bmatrix} \boldsymbol{r} \\ \boldsymbol{u} \\ \boldsymbol{a}_e \end{bmatrix}$$

The differential equations (14) and (15) may be expressed by

$$\overset{I}{\boldsymbol{x}} = F(t)\boldsymbol{x} + \boldsymbol{f}(t)$$

$$F(t) = \begin{bmatrix} O_3 & I_3 & O_3 \\ \Gamma_p & O_3 & I_3 \\ O_3 & O_3 & \beta_e I_3 \end{bmatrix}, \qquad O_3 = \begin{bmatrix} 0 & 0 & 0 \\ 0 & 0 & 0 \\ 0 & 0 & 0 \end{bmatrix}$$

$$I_3 = \begin{bmatrix} 1 & 0 & 0 \\ 0 & 1 & 0 \\ 0 & 0 & 1 \end{bmatrix} \tag{16}$$

$$\boldsymbol{f}(t) = \begin{bmatrix} \boldsymbol{0} \\ -\boldsymbol{a}_p \quad -\boldsymbol{a}_c \\ \boldsymbol{0} \end{bmatrix}, \qquad \boldsymbol{0} = \begin{bmatrix} 0 \\ 0 \\ 0 \end{bmatrix}$$

where the 3×3 matrix Γ_p depends implicitly on $\boldsymbol{r}_p$. The vectors $\boldsymbol{r}_p(t), \boldsymbol{f}(t)$ may be determined from the outputs of the pursuer inertial-navigation system (INS). As $\boldsymbol{r}_p, \boldsymbol{f}$ do not participate in the filtering process, the filter equations (16) are linear with respect to $\boldsymbol{x}$, with time-dependent coefficients.

V. Nonlinear Estimation Algorithm

Several techniques for nonlinear estimation include minimum-variance estimation, estimation by statistical linearization, and least-squares estimation.[11] The minimum-variance technique is implemented because of its simplicity, from a computational standpoint, compared to the other two methods.

The simplest form of the minimum-variance estimator is the extended Kalman filter (EKF). The EKF generates estimates of the state vector $\hat{\boldsymbol{x}}$ from measurements z. Measurements are nonlinear functions of the true state $\boldsymbol{x}$, corrupted by additive errors with Gaussian statistical properties:

$$z = \boldsymbol{h}(\boldsymbol{x}) + \nu, \qquad \mathcal{E}\{\nu\} = 0, \qquad \mathcal{E}\{\nu\nu^T\} = R$$

where R is the measurement-noise covariance matrix.

The EKF consists of equations that specify the state estimate $\hat{\boldsymbol{x}}$ and certain auxiliary equations that specify the filter-covariance matrix P. As measurements z_i are available at discrete times $t = t_i$, the EKF update equations may be implemented:

$$\hat{\boldsymbol{x}}_i(+) = \hat{\boldsymbol{x}}_i(-) + K_i[z_i - \boldsymbol{h}(\hat{\boldsymbol{x}}_i(-))] \tag{17a}$$

$$K_i = P_i(-)H_i^T(-)\left[H_i(-)P_i(-)H_i^T(-) + R_i\right]^{-1} \tag{17b}$$

$$P_i(+) = [I - K_i H_i(-)]P_i(-) \tag{17c}$$

where $(-)$ indicates the value immediately before the update and $(+)$ indicates the value immediately after the update. Referring to Eq. (17), the estimates are updated with the nonlinear measurement function $\boldsymbol{h}(\boldsymbol{x})$, whereas the EKF gains K_i depend on the measurement-sensitivity matrix $H = \partial \boldsymbol{h}/\partial \boldsymbol{x}$, evaluated at $\boldsymbol{x} = \hat{\boldsymbol{x}}_i(-)$.

Between successive updates, a linear dynamic system, based on Eq. (16) may be integrated forward to the next update

$$\frac{\mathrm{d}\hat{\boldsymbol{x}}}{\mathrm{d}t} = F(t)\hat{\boldsymbol{x}} + \boldsymbol{f}(t), \qquad \dot{P} = F(t)P + PF^T(t) \tag{18}$$

where $\hat{\boldsymbol{x}}_i(+)$ and $P_i(+)$ are initial conditions. The solutions of these equations specify $\hat{\boldsymbol{x}}_{i+1}(-)$ and $P_{i+1}(-)$, just prior to the update at $t = t_{i+1}$. The matrix $F(t)$ and vector $\boldsymbol{f}(t)$ depend on the outputs of the pursuer INS (refer to Sec. IV). In reality, these quantities will contain small errors arising from INS instrumentation errors and misalignment angles. These effects are not included here.

Measurements from a body-fixed (strapdown) seeker may be mathematically modeled as the spherical-polar angles of the line-of-sight vector $\boldsymbol{r}$:

$$h_1 = \tan^{-1}\frac{y_2}{y_1}, \qquad h_2 = \tan^{-1}\frac{y_3}{y_{12}} \qquad (19)$$
$$y_{12} = \sqrt{y_1^2 + y_2^2}$$

The components of $\boldsymbol{r}$ in body axes may be expressed by linear functions of the first three state variables:

$$\begin{bmatrix} y_1 \\ y_2 \\ y_3 \end{bmatrix} = \mathcal{R}\begin{bmatrix} x_1 \\ x_2 \\ x_3 \end{bmatrix}$$

where x_1, x_2, x_3 are the components of $\boldsymbol{r}$ in the inertial frame. The measurement-sensitivity matrix H is a rectangular 2×9 matrix:

$$H(\boldsymbol{x}) = \frac{\partial(h_1, h_2)}{\partial(x_1, x_2, x_3, x_4, x_5, x_6, x_7, x_8, x_9)}$$

Nonzero elements of H are contained in a 2×3 submatrix:

$$\frac{\partial(h_1, h_2)}{\partial(x_1, x_2, x_3)} = \frac{\partial(h_1, h_2)}{\partial(y_1, y_2, y_3)}\frac{\partial(y_1, y_2, y_3)}{\partial(x_1, x_2, x_3)}$$

$$\frac{\partial(h_1, h_2)}{\partial(y_1, y_2, y_3)} = \begin{bmatrix} -\dfrac{y_2}{y_{12}^2} & \dfrac{y_1}{y_{12}^2} & 0 \\ -\dfrac{y_1 y_3}{y_{12} y^2} & -\dfrac{y_2 y_3}{y_{12} y^2} & \dfrac{y_{12}}{y^2} \end{bmatrix}$$

$$\frac{\partial(y_1, y_2, y_3)}{\partial(x_1, x_2, x_3)} = \mathcal{R}$$

where $y^2 = y_1^2 + y_2^2 + y_3^2$ and $\mathcal{R}$ is the rotation matrix from the inertial frame to the pursuer body frame.

VI. Monte Carlo Simulation

For the EKF, the filter-covariance matrix P is the lowest order approximation of the true state-error covariance matrix because nonlinear expectations are approximated by the lowest order terms of a series expansion about the current estimate.[11] As nonlinear effects may generate non-Gaussian statistics for the output variables, P may not accurately characterize EKF performance. Examples of nonlinearities include saturation limits and deadbands in control systems.

Monte Carlo simulation of the EKF and its nonlinear truth model provide the highest confidence level for evaluation of performance of the guidance and estimation algorithms. In pursuit-evasion guidance simulation (PEGS), both vehicles are modeled by dynamic systems with six degrees of freedom. Aerodynamic forces and moments are specified using different sets of aerodynamic coefficients for each vehicle. For the pursuer vehicle, additional degrees of freedom model the EKF, the control-actuation process, and variable mass and inertia properties associated with propulsion.

The EKF state estimates and filter-covariance matrix are updated using Eq. (17), with measurements synthesized from the deterministic truth model. At each EKF update, true line-of-sight angles are corrupted with randomly sampled errors whose statistical properties are consistent with the EKF measurement model. An additional 54 variables model the differential equation (18) that propagate the state estimate and error-covariance matrix between updates.

Translational accelerations are generated by four independently controlled thrusters in the vehicle yz plane, located near the pursuer mass center. Commands to these thrusters are thrust saturation limited, and the actuation process is modeled by a first-order lag with time constant 5 ms. Thrust commands are generated by transforming the optimal control (6) from inertial to pursuer body axes:

$$\tilde{\boldsymbol{a}}_c^* = \mathcal{R}\hat{\boldsymbol{a}}_c^*, \qquad \hat{\boldsymbol{a}}_c^* = \frac{3}{\hat{\tau}^2}\left[\hat{\boldsymbol{r}} + \hat{\tau}\hat{\boldsymbol{u}} + \tfrac{1}{2}\hat{\tau}^2\hat{\boldsymbol{a}}_d\right]$$

$$\hat{\boldsymbol{a}}_d = \hat{\boldsymbol{a}}_e - \boldsymbol{a}_p$$

where $\hat{\boldsymbol{r}}, \hat{\boldsymbol{u}}, \hat{\boldsymbol{a}}_e$ are the EKF estimates in the inertial frame. Estimated time to go $\hat{\tau}$ is selected to generate a zero value of the body x-axis component of $\tilde{\boldsymbol{a}}_c^*$. Using a formula similar to Eq. (8), $\hat{\tau}$ is specified using current EKF estimates, transformed to the body frame. These calculations are repeated at each guidance command update, until three actuation time constants before predicted intercept, corresponding to $\hat{\tau} = 15$ ms.

Attitude-control torques are generated by six independently controlled thrusters in the vehicle base plane. Thrust commands are generated by an autopilot algorithm that stabilizes the vehicle near zero angle of attack. Actuation lags (time constant 5 ms) and thrust saturation limits are included.

In the Monte Carlo mode, the deterministic model is initialized with randomly selected parameters. Initial conditions and constant parameters are selected once, at the beginning of a trial. Initial values are specified for the state vectors of each vehicle and the EKF statistics. EKF statistics consist of the mean and covariance matrix of the relative-position vector, relative-velocity vector, and evader acceleration vector. EKF statistics are consistent with the actual statistics for each vehicle, as follows.

The evader state vector is specified by the position, velocity, and angular rate vectors and three Euler angles that define vehicle orientation relative to inertial space. It is assumed that evader position and velocity are updated once, by a ground-based radar. Initial position and velocity errors are conservatively large, isotropic in all axes, and uncorrelated (refer to Table 1). (In reality, uncertainties will be much smaller along the radar slant range, compared to angular directions.) Uncorrelated position errors make the in-flight estimation process more difficult, because range errors cannot be observed with angle measurements.

As the radar update does not specify evader attitude directly, it is assumed that misalignment angles between the longitudinal axis and Earth relative velocity vector are very small (0.01 deg). For a spin-stabilized evader, small angles of attack suppress disturbances caused by helical motions about the velocity vector, which are not modeled in the EKF. Small angular rate errors (0.1 deg/s) are also assumed.

Pursuer position, velocity, attitude, and angular rate statistics are derived by covariance analysis techniques. An initial covariance matrix is specified at launch, reflecting the accuracies of the INS erection, alignment, and initialization processes during the prelaunch phase. This covariance matrix is propagated from the launch point, along theoretical boost and midcourse trajectories, to the point where the endgame segment begins. Instrument errors are modeled by zero-mean bias states, with uncertainties specified by an error coefficient model. At endgame initiation, pursuer position and velocity uncertainties are comparable to corresponding evader uncertainties (refer to Table 1).

EKF statistics combine position and velocity statistics of each vehicle and the statistics of the evader acceleration (refer to Table 2). All vectors are resolved in an Earth-centered inertial (ECI) frame. Evader acceleration statistics are determined by its position, velocity, attitude statistics, and nominal values of atmospheric, aerodynamic, and configurational parameters. Evader attitude statistics determine initial angle of attack, which modulates lift and drag accelerations.

The three components of $\vec{a}_e$ have small uncertainties compared to their mean values at $t = 0$. Much larger uncertainties would occur, for example, at larger angles of attack and for off-nominal values of the atmospheric parameters and ballistic coefficient. Atmospheric parameters may have uncertainties as large as 4–10%

Table 1 Initial standard deviations for pursuer and evader

Parameter	ECI[a] state	Standard deviation	
		Evader	Pursuer
Inertial position component, m	X	50.0	26.7
	Y	50.0	28.9
	Z	50.0	22.2
Inertial velocity component, m/s	$\dot{X}$	5.0	1.62
	$\dot{Y}$	5.0	1.80
	$\dot{Z}$	5.0	1.34

[a]Components in Earth-centered inertial (ECI) coordinates.

Table 2 Initial statistics for EKF at two crossing angles

Parameter	EKF[a] state	10 deg crossing angle Mean value	10 deg crossing angle 1σ value	90 deg crossing angle Mean value	90 deg crossing angle 1σ value
Relative position component, m	x_1	7,204	55.9	7,202	53.9
	x_2	−18,778	56.4	−6,472	56.4
	x_3	−2	55.1	10,852	55.1
Relative velocity component, m/s	x_4	−3,696.3	5.37	−3,695.4	5.37
	x_5	9,716.5	5.26	3,536.1	5.26
	x_6	0.1	5.38	−5,450.9	5.38
Evader acceleration component, m/s^2	x_7	8.47	0.148	8.47	0.140
	x_8	−18.30	0.153	2.29	0.074
	x_9	0.00	0.144	18.16	0.154

[a]Components in ECI coordinates.

of their nominal values at altitudes above 25 km. Uncertainties in the evader ballistic coefficient may be appreciable when the vehicle configuration is unknown. These uncertainties were not included in the present evaluation.

VII. Performance of Filter

When target dynamics are not well characterized, Kalman tracking filters diverge because target acceleration states are not completely observable with angle measurements.[9,17,19] This problem is aggravated for sudden or complicated maneuvers, and an adaptive filtering approach is often suggested.

In the present application, an adaptive filtering approach was not needed because the EKF did not diverge, for the following reasons: 1) very accurate angle measurements and high update rates, 2) "self-consistent" initialization of the EKF, and 3) accurate model of target acceleration.

Small angular uncertainty σ_θ and high update rate f minimize uncertainty in estimated position in a direction normal to the line of sight:

$$\sigma_n(t) \cong r(t)\frac{\sigma_\theta}{\sqrt{1+ft}} \qquad (t \geq 0) \tag{20}$$

where $r(t)$ is the instantaneous range. With filtering, better accuracy may be achieved by increasing the total number of measurements $(1 + ft)$.

"Self-consistent" initialization of the EKF means that initial conditions of the EKF are consistent with the sets of state vector statistics for each vehicle at $t = 0$ (refer to Tables 1 and 2). For the unobservable states, the EKF relies on its own covariance predictions to update the estimates.

Finally, over a limited time interval (2 s), an exponential acceleration model tracks the exponential increase in mean drag, provided the target angle of attack is small. Acceleration errors show a sinusoidal oscillation at frequency 5 Hz, corresponding to the helical motion of the target mass center associated with aerodynamic lift. It is anticipated that additional filter states and high update rates ($10 < f < 50$ Hz) will be needed to track these oscillations.

These considerations explain why actual errors in the estimates were reasonably consistent with the corresponding EKF filter covariance predictions. With angle measurements, the EKF quickly reduces errors perpendicular to the pursuer-to-evader range direction (refer to Fig. 1). Uncertainties in these states may be approximated by Eq. (20). Errors along the pursuer-to-evader range direction are large and unobservable for most of the engagement. During the last 50 ms before intercept, rapid motion of the line-of-sight vector increases the observability of range errors. High update rates are necessary to track these dynamics, and fast response times are desirable to implement last-second corrections to the trajectory.

Errors in the EKF estimates of range are considerably larger than actual miss distances. Miss distance is determined by the error in the estimate of the zero-effort miss vector $\hat{\boldsymbol{r}}(\hat{T})$ at the estimated final time $\hat{T}$. During an engagement, this vector may be determined from EKF estimates:

$$\hat{\boldsymbol{r}}(\hat{T}) = \hat{\boldsymbol{r}} + \hat{\tau}\hat{\boldsymbol{u}} + \tfrac{1}{2}\hat{\tau}^2(\hat{\boldsymbol{a}}_e - \boldsymbol{a}_p), \qquad \hat{T} = \hat{\tau} + t$$

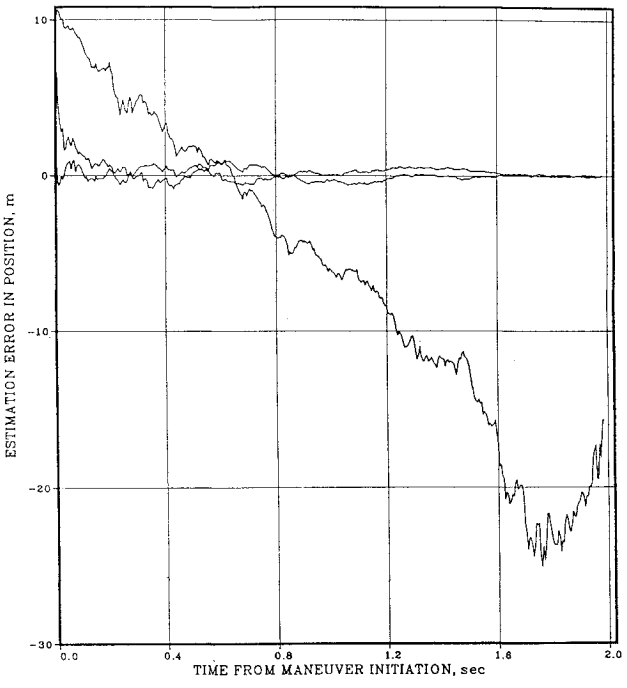

Fig. 1 Estimation errors in range are large compared to errors normal to line of sight (measurement accuracy 0.2 mrad, EKF update rate 200 Hz, and crossing angle 10 deg).

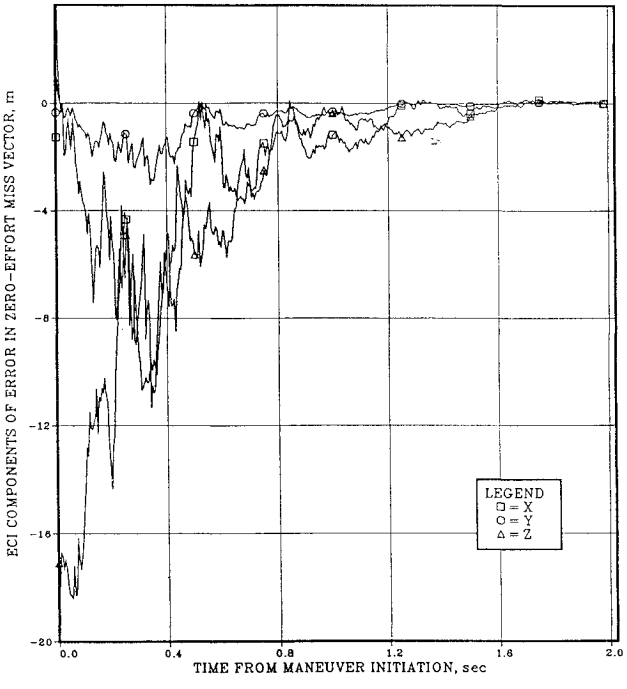

Fig. 2 Errors in zero effort miss vector converge, despite large errors in EKF estimates of range (measurement accuracy 0.2 mrad, EKF update rate 200 Hz, crossing angle 10 deg).

where $\hat{\tau}$ is specified with EKF estimates (refer to Sec. III). The error in the estimate may be approximated by

$$\delta\hat{\boldsymbol{r}}(\hat{T}) = \delta\hat{\boldsymbol{r}} + \hat{\tau}\delta\hat{\boldsymbol{u}} + \tfrac{1}{2}\hat{\tau}^2\delta\hat{\boldsymbol{a}}_e + [\hat{\boldsymbol{u}} + (\hat{\boldsymbol{a}}_e - \boldsymbol{a}_p)\hat{\tau}]\delta\hat{T} \tag{21}$$

where $\delta\hat{\boldsymbol{r}}$, $\delta\hat{\boldsymbol{u}}$, $\delta\hat{\boldsymbol{a}}_e$ are the errors in the EKF estimates, and $\delta\hat{T}$ is the error in final time caused by errors in EKF estimates. Although certain components of $\delta\hat{\boldsymbol{r}}$ can be large, compensating errors in $\delta\hat{\boldsymbol{u}}$ and $\delta\hat{T}$ reduce the component magnitudes of $\delta\hat{\boldsymbol{r}}(\hat{T})$ (refer to Fig. 2).

Compensating errors $\delta\hat{T}$ are generated by the time-to-go algorithm when filter states are used. For example, when time to go is computed with a fixed final time T (rather than $\hat{T}$), the error vector may be approximated by

$$\delta\hat{r}(T) = \delta\hat{r} + (T - t)\delta\hat{u} + \tfrac{1}{2}(T - t)^2\delta\hat{a}_e \qquad (22)$$

As there are no compensating errors in final time in Eq. (22), the components of Eq. (22) are two orders of magnitude larger than the components of Eq. (21).

VIII. Theoretical Limits on Accuracy

Theoretical limits on accuracy were determined with the PEGS simulation in Monte Carlo mode. The results represent the best accuracy that might be achieved because of the approximations and simplifications described earlier (refer to Sec. VI). Nonetheless, the trends are useful in specifying requirements on measurement accuracy and update rate for the seeker. Moreover, the results demonstrate the effectiveness of the guidance and filtering algorithms in achieving successful intercepts.

Several engagement geometries were evaluated, with different "crossing angles," measured between the Earth-relative velocity vectors of each vehicle at the nominal intercept point. As the nominal time of flight is always the same (2 s), the largest initial range (20.1 km) and closing velocity (−10.4 km/s) occur at the smallest crossing angle (10 deg). At the largest crossing angle (90 deg), the smallest initial range (14.5 km) and closing velocity (−7.5 km/s) occur. Tail-chase engagements were not considered because $v_p < v_e$.

In the simulation, the closest approach distance $r_{\min}$, measured between the vehicle centers of mass, was determined accurately by carefully reducing the integration step size Δt. At small separation distances ($r < 1$ m), Δt is a fraction of the smaller of two "characteristic times" τ_r, τ_θ:

$$\Delta t = \tfrac{1}{10}\min\{\tau_r, \tau_\theta\}, \qquad \tau_r = (r/\dot{r}), \qquad \tau_\theta = (\theta/\dot{\theta})$$

Initially, line-of-sight angle θ does not change rapidly ($\tau_r \ll \tau_\theta$). Near closest approach, θ changes rapidly ($\tau_\theta \ll \tau_r$).

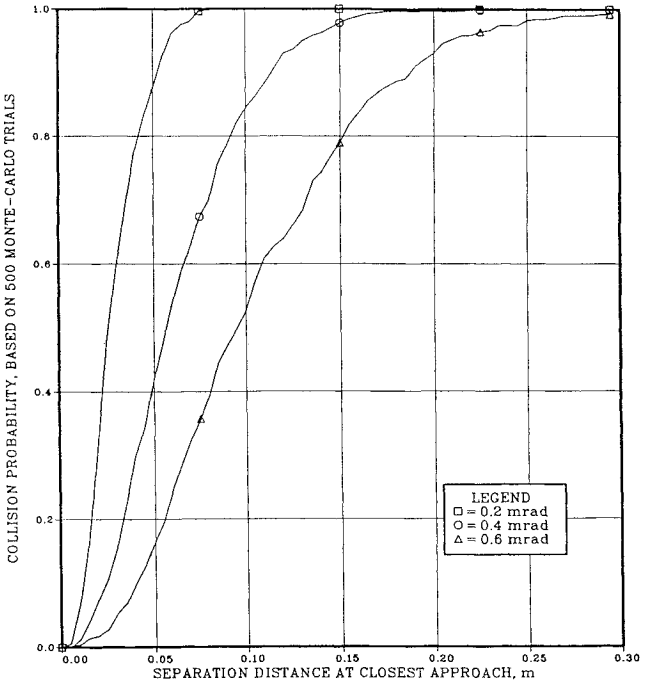

Fig. 3 Theoretical limits on collision probability for different measurement accuracies (seeker EKF update rate 200 Hz, crossing angle 10 deg).

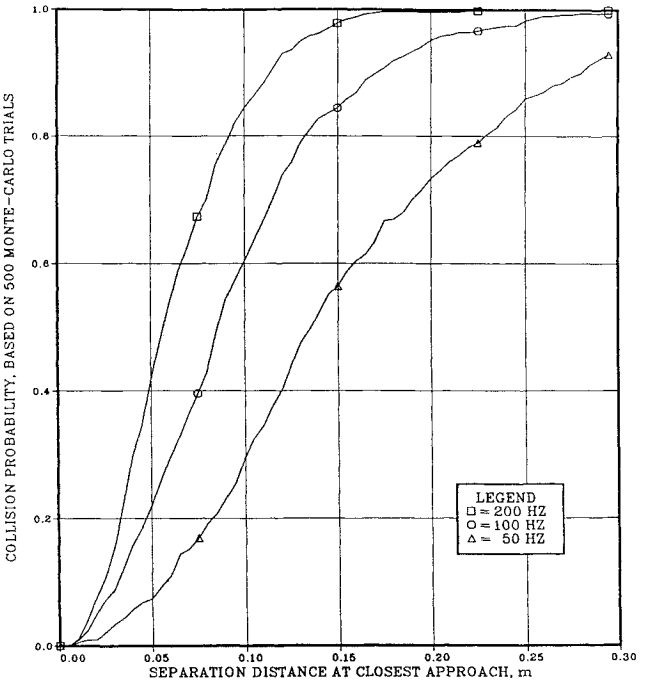

Fig. 4 Theoretical limits on collision probability for different seeker EKF update rates (measurement accuracy 0.4 mrad, crossing angle 10 deg).

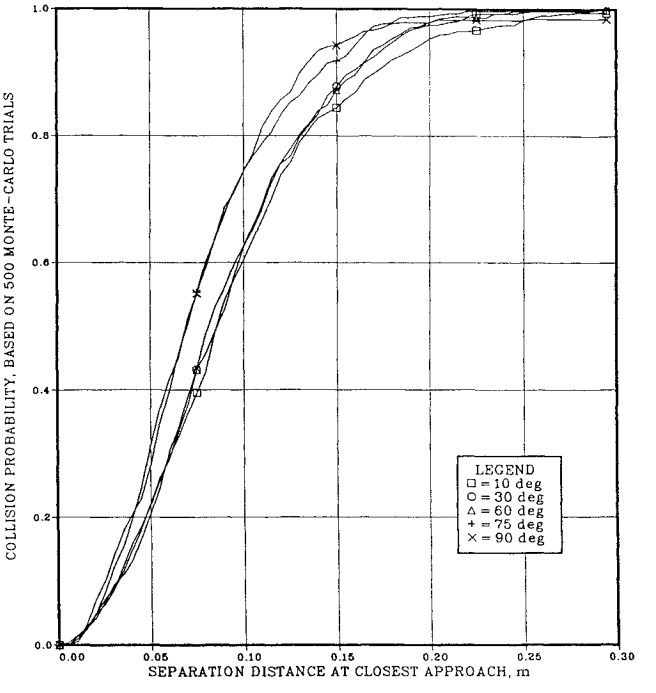

Fig. 5 Theoretical limits on collision probability for engagements with different crossing angles (measurement accuracy 0.4 mrad, update rate 100 Hz).

The performance measure of accuracy was the collision probability

$$p(r) = (n(r)/N), \qquad r_{\min} \le r$$

where n is the number of trials for which $r_{\min}$ is smaller than a specified separation distance r. The total number of Monte Carlo trials is $N = 500$.

Monte Carlo results indicate that $p(r)$ is strongly dependent on the measurement accuracy σ_θ of the line-of-sight angle and the EKF update rate f. At a fixed f value, p increases as σ_θ decreases (refer to Fig. 3). At a fixed σ_θ value, p increases as f increases (refer to Fig. 4).

The worst accuracy occurs at the smallest crossing angle (10 deg) because slant range is relatively unobservable with angle-only measurements. As crossing angle increases, collision probability generally increases (refer to Fig. 5). At the largest crossing angle (90 deg), there is better correlation between errors in range and angle, and smaller estimation errors in range may be achieved.

IX. Conclusions

In this article, optimal-guidance and nonlinear estimation algorithms are formulated for interception of a nonmaneuvering target vehicle decelerated by atmospheric drag. Two contributions are concerned with 1) a new algorithm for specifying time to go, which has surprising advantages from a filtering standpoint, and 2) a new EKF model for target mean deceleration.

An optimal-guidance algorithm is formulated for three-axis control of translational acceleration, with perturbations arising from a variable disturbing acceleration. With two-axis control, time to go may be selected to generate a zero-acceleration command along the uncontrolled axis. This technique shifts the aimpoint along the evader trajectory, increasing control effectiveness and estimation accuracy.

A nine-state EKF is formulated in a Cartesian-inertial frame. The states include the relative-position vector, relative-velocity vector, and absolute-acceleration vector of the evader vehicle. Over short time intervals, the target deceleration vector may be approximated by a linear, first-order process. The EKF dynamics model is linear in the state variables. Seeker-angle measurements are nonlinear functions of the state variables.

Statistical properties of the EKF are evaluated by Monte Carlo simulation of the EKF and its nonlinear truth model. Although certain states are unobservable with angle measurements, filter estimates do not diverge because of very accurate angle measurements, high update rates of the EKF, self-consistent initialization of the EKF, and a good model of target deceleration. Surprisingly, very small miss distances can be achieved, despite large estimation errors in range, because of the time-to-go algorithm.

Theoretical limits on collision probability are determined by Monte Carlo simulation. Based on 500 Monte Carlo trials per case, collision probability is strongly dependent on measurement accuracy of the line-of-sight angle, EKF update rate, and trajectory crossing angle. At a specified separation distance, the largest collision probabilities occur for the most accurate measurements, highest update rates, and perpendicular crossing geometries.

Appendix: Optimal-Guidance Algorithm

An optimal-guidance algorithm is derived using the calculus of variations. The dynamic system is specified in relative-motion coordinates:

$$\overset{I}{\boldsymbol{u}} = -\boldsymbol{a}_c + \boldsymbol{a}_d, \qquad \overset{I}{\boldsymbol{r}} = \boldsymbol{u}$$

where $\boldsymbol{a}_c$ is the (pursuer) acceleration-control vector, and $\boldsymbol{a}_d$ is a variable disturbance acceleration. The cost function may be expressed by the sum of three independent cost functions J_i:

$$J = \sum_{i=1}^{3} J_i, \qquad J_i = \tfrac{1}{2} b r_i^2(T) + \frac{1}{2c}\int_0^T a_{c,i}^2 \, \mathrm{d}t$$

where T is the final time and $r_i, a_{c,i}$ are the components of $\boldsymbol{r}, \boldsymbol{a}_c$, respectively. The constants b, c are "weighting factors" on terminal miss and control effort, respectively.

As the equations of motion and cost function are separable, three optimization problems may be solved independently. For each control axis, the equations of motion and cost function may be expressed by

$$\dot{u} = -a_c + a_d, \qquad \dot{r} = u \tag{A1}$$

$$J = \tfrac{1}{2} b r^2(T) + \frac{1}{2c}\int_0^T a_c^2 \, \mathrm{d}t \tag{A2}$$

where subscripts i have been omitted for notational brevity.

The Hamiltonian function is specified by adjoining the dynamic equations (A1) to the cost function (A2):

$$\mathcal{H} = \frac{1}{2}\frac{a_c^2}{c} + \lambda u + \nu(-a_c + a_d)$$

Lagrange-multiplier functions λ, ν are specified by the adjoint equations

$$\dot{\lambda} = -\frac{\partial \mathcal{H}}{\partial r} = 0, \qquad \dot{\nu} = -\frac{\partial \mathcal{H}}{\partial u} = -\lambda \tag{A3}$$

"Initial" conditions are specified at the final time:

$$\lambda(T) = \frac{\partial J}{\partial r(T)} = b r(T), \qquad \nu(T) = \frac{\partial J}{\partial u(T)} = 0 \tag{A4}$$

The solutions of Eq. (A3), with final conditions (A4) may be expressed by

$$\lambda(t) = \lambda(T), \qquad \nu(t) = b r(T)(T - t) \tag{A5}$$

The necessary condition for optimality specifies the optimal control:

$$\frac{\partial \mathcal{H}}{\partial a_c} = \frac{a_c}{c} - \nu = 0, \qquad a_c^*(t) = c\nu(t)$$

Following substitution of Eq. (A5), it follows that

$$a_c^*(t) = \omega(T - t), \qquad \omega = bcr(T) \tag{A6}$$

The optimal control (A6) may be specified in "feedback form" by expressing $r(T)$ as a function of the state variables at the current time. For this purpose, the dynamic equations (A1) may be integrated backward from $t = T$ to the current time t after the independent variable is changed from t to $\tau = T - t$:

$$\frac{\mathrm{d}r}{\mathrm{d}\tau} = -u, \qquad \frac{\mathrm{d}u}{\mathrm{d}\tau} = a_c^*(\tau) - a_d(\tau), \qquad a_c^*(\tau) = \omega\tau$$

The solutions of this system may be expressed by

$$u(\tau) = u(T) + \tfrac{1}{2}\omega\tau^2 - \eta(\tau), \qquad \eta(\tau) = \int_0^\tau a_d(s)\, \mathrm{d}s$$

$$r(\tau) = r(T) - u(T)\tau - \tfrac{1}{6}\omega\tau^3 + \rho(\tau), \qquad \rho(\tau) = \int_0^\tau \eta(s)\, \mathrm{d}s$$

where $\tau = 0$ corresponds to $t = T$. The solutions may be combined to specify

$$r(T) = \frac{r(\tau) + \tau u(\tau) + \tau\eta(\tau) - \rho(\tau)}{1 + \frac{1}{3}bc\tau^3} \tag{A7}$$

Following substitution of Eq. (A7) in Eq. (A6), it follows that

$$a_c^*(\tau) = K(\tau)[r(\tau) + \tau u(\tau) + \tau\eta(\tau) - \rho(\tau)]$$

$$K(\tau) = \frac{3bc\tau}{3 + bc\tau^3} \tag{A8}$$

As the same solution (A8) applies to all three control axes, the complete solution may be generalized to the following vector form:

$$\boldsymbol{a}_c^*(\tau) = K(\tau)[\boldsymbol{r}(\tau) + \tau\boldsymbol{u}(\tau) + \tau\boldsymbol{\eta}(\tau) - \boldsymbol{\rho}(\tau)]$$

$$K(\tau) = \frac{3bc\tau}{3 + bc\tau^3}, \qquad \boldsymbol{\eta}(\tau) = \int_0^\tau \boldsymbol{a}_d(s)\, \mathrm{d}s$$

$$\boldsymbol{\rho}(\tau) = \int_0^\tau \boldsymbol{\eta}(s)\, \mathrm{d}s$$

By repeated applications of the rule of integration by parts, these quadratures may be replaced by power-series expansions in τ, with coefficients depending on the derivatives of the integrands:

$$\eta(\tau) = \sum_{q=1}^{N} \frac{(-1)^{q-1}}{q!} \tau^q \frac{\mathrm{d}^{q-1}\boldsymbol{a}_d}{\mathrm{d}\tau^{q-1}} - \frac{(-1)^N}{N!} \eta_N(\tau)$$

$$\rho(\tau) = \sum_{q=1}^{N} \frac{(-1)^{q-1}}{q!} \tau^q \frac{\mathrm{d}^{q-1}\eta}{\mathrm{d}\tau^{q-1}} - \frac{(-1)^N}{N!} \rho_N(\tau)$$

$$\eta_N(\tau) = \int_0^\tau s^N \frac{\mathrm{d}^N \boldsymbol{a}_d}{\mathrm{d}\tau^N}\,\mathrm{d}s, \qquad \rho_N(\tau) = \int_0^\tau s^N \frac{\mathrm{d}^N \eta}{\mathrm{d}\tau^N}\,\mathrm{d}s$$

References

[1]Schindler, R., "SDI Thinks Small," *Aerospace America,* April 1990, pp. 22–25.

[2]Spencer, A., and Moore, W., "Design Trade-Offs For Homing Missiles," AIAA Paper 92-2755, May 1992.

[3]Bryson, A., and Ho, Y., *Applied Optimal Control,* Ginn and Co., New York, 1969.

[4]Hull, D., Radke, J., and Mack, R., "Time-to-Go Prediction for Homing Missiles Based on Minimum-Time Intercepts," *Journal of Guidance, Control, and Dynamics,* Vol. 14, No. 5, 1991, pp. 865–871.

[5]Lee, G. K. F., "Estimation of the Time-to-Go Parameter for Air-to-Air Missiles," *Journal of Guidance, Control, and Dynamics,* Vol. 8, No. 2, 1985, pp. 262–266.

[6]Becker, K., "Closed-Form Solution of Pure Proportional Navigation," *IEEE Transactions on Aerospace and Electronic Systems,* Vol. 26, No. 3, 1990, pp. 526–533.

[7]Guelman, M., "The Closed-Form Solution of True Proportional Navigation," *IEEE Transactions on Aerospace and Electronic Systems,* Vol. AES-12, No. 4, 1976, pp. 472–482.

[8]Murtaugh, S., and Criel, H., "Fundamentals of Proportional Navigation," *IEEE Spectrum,* Dec. 1966, pp. 75–85.

[9]Guelman, M., "Proportional Navigation with a Maneuvering Target," *IEEE Transactions on Aerospace and Electronic Systems,* Vol. AES-8, No. 3, 1972, pp. 364–371.

[10]Mahapatra, P., and Shukla, U., "Accurate Solution of Proportional Navigation for Maneuvering Targets," *IEEE Transactions on Aerospace and Electronic Systems,* Vol. AES-25, No. 1, 1989, pp. 81–89.

[11]Gelb, A., Kasper, J., Nash, R., Price, C., and Sutherland, A., *Applied Optimal Estimation,* MIT Press, Cambridge, MA, 1974.

[12]Jazwinski, A., *Stochastic Processes and Filtering Theory,* Academic, New York, 1970.

[13]Hepner, S., and Geering, H., "Observability Analysis for Target Maneuver Estimation via Bearing-Only and Bearing-Rate-Only Measurements," *Journal of Guidance, Control, and Dynamics,* Vol. 13, No. 6, 1990, pp. 977–983.

[14]Hepner, S., and Geering, H., "Adaptive, Two-Time-Scale Tracking Filter for Target Acceleration Estimation," *Journal of Guidance, Control, and Dynamics,* Vol. 14, No. 3, 1991, pp. 581–588.

[15]Lindgren, A., and Gong, K., "Position and Velocity Estimation Via Bearing Observations," *IEEE Transactions on Aerospace and Electronic Systems,* Vol. AES-14, No. 4, 1978, pp. 564–577.

[16]Tenney, R., Hebbert, R., and Sandell, N., "A Tracking Filter for Maneuvering Sources," *IEEE Transactions on Automatic Control,* April 1977, pp. 246–251.

[17]Aidala, V., "Kalman Filter Behavior in Bearings-Only Tracking Applications," *IEEE Transactions on Aerospace and Electronic Systems,* Vol. AES-15, No. 1, 1979, pp. 29–39.

[18]Nardone, S., and Aidala, V., "Observability Criteria for Bearings-Only Target Motion Analysis," *IEEE Transactions on Aerospace and Electronic Systems,* Vol. AES-17, No. 2, 1981, pp. 162–166.

[19]Weiss, H., and Moore, J., "Improved Extended Kalman Filter Design for Passive Tracking," *IEEE Transactions on Automatic Control,* Vol. AC-25, No. 4, 1980, pp. 807–811.